ISSN 0915-633X

NATIONAL INSTITUTE FOR FUSION SCIENCE

Design of Spheromak Injector Using Conical Accelerator for Large Helical Device

J. Miyazawa, H. Yamada, K. Yasui, S. Kato, N., Fukumoto,
M. Nagata and T. Uyama

(Received - Nov. 8, 1999)

NIFS-614 Nov. 1999

RESEARCH REPORT
NIFS Series

NAGOYA, JAPAN

Design of Spheromak Injector using Conical Accelerator for Large Helical Device

J. Miyazawa[a] *, H. Yamada[a], K. Yasui[a], S. Kato[a], N. Fukumoto[b], M. Nagata[b], and T. Uyama[b]
a. National Institute for Fusion Science, Toki, Gifu 509-5292, Japan
b. Himeji Institute of Technology, Himeji, Hyogo 671-2201, Japan
* corresponding author: email miyazawa@LHD.nifs.ac.jp

Abstract

Optimization of CT injector for LHD has been carried out and conical electrode for adiabatic CT compression is adopted in the design. Point-model of CT acceleration in a co-axial electrode is solved to optimize the electrode geometry and the power supplies. Large acceleration efficiency of 34 % is to be obtained with 3.2 m long conical accelerator and 40 kV - 42 kJ power supply. The operation scenario of a CT injector named SPICA mk. I (SPheromak Injector using Conical Accelerator) consisting of 0.8 m conical accelerator is discussed based on this design.

Keywords: Compact Toroid, LHD, acceleration efficiency, conical accelerator, adiabatic compression

1. Introduction

Compact toroid (CT) injection is a new fueling method that is capable of central fueling into hot fusion plasmas [1-3]. Conventional fueling methods such as gas puffing and ice-pellet injection are not adequate for deep fueling because neutral particles injected into hot plasmas are ionized immediately and the subsequent penetration is shallow. Cold neutrals also cause the loss of hot particles through the charge exchange reaction, and high fueling efficiency is not expected. CT is a dense magnetized plasmoid and can be easily accelerated over hundreds of km/s by the electro-magnetic force [4-8]. A high-speed CT can penetrate into the hot main plasma that is confined in the strong magnetic field and thus the center fueling is achievable [9-11]. The peaked density profile obtained after the center fueling is favorable because the density gradient causes the rotation of plasmas. The rotation of fusion plasma is indispensable to achieve the high-confinement condition [12-17]. The large momentum carried by the high-speed CT is also useful to rotate the main plasma.

Spheromak is one of CT configurations where both of the toroidal- and poloidal-magnetic fields are generated and sustained by currents flowing only inside the spheromak itself [18]. This CT is usually formed using a co-axial magnetized plasma gun, and accelerated by another co-axial accelerator connected to the formation electrode. In the accelerator part, the radial current flowing between the inner- and the outer-electrode accelerates the CT with its $\boldsymbol{J}\times\boldsymbol{B}$ force. High-energy capacitor banks supply the accelerator with the radial current and the CT kinetic energy is in proportion to the bank energy in general. A CT injected into the magnetically confined fusion plasmas suffers from the repelling force due to the gradient of magnetic field strength $\nabla \boldsymbol{B}^2$ [19-21]. Therefore, sufficient kinetic energy that is comparable to the magnetic potential energy $V_{CT}B^2/(2\mu_0)$ (V_{CT}: CT volume) is necessary to inject the CT deep inside the strong magnetic field. CT kinetic energy of more than 15 kJ should be supplied to inject a spherical CT of 0.1 m radius into 3 T magnetic field, for instance. The ratio of CT kinetic energy to the bank energy is defined as the acceleration efficiency ε. High efficiency is required to reduce the total cost of a CT injector that largely depends on the capacitor bank energy. It is shown in this paper that ε is a function of L/L_{ext} (where L is the inductance of the co-axial accelerator, L_{ext} is the external inductance of the acceleration circuit). Large L and/or small L_{ext} are favorable to attain large ε. The ratio R_{out}/R_{in} (R_{in}: the inner-electrode radius, and R_{out} the outer-electrode radius) and the electrode length l determine L. When R_{out}/R_{in} and/or l are large, L is also large.

The lifetime of a CT τ_{CT} is one of the important parameters especially in the large reactor-sized devices such as ITER (International Thermonuclear Experiment Reactor) and LHD (Large Helical Device) [22, 23]. As the distance from the injection port to the main plasma is long, the time-of-flight is expected to be long comparable to τ_{CT} of a usual CT in these large devices. For the case of dense and low-temperature CT, τ_{CT} is determined by the resistive decay as $\tau_{CT} \sim \mu_0/(\lambda^2\eta)$, where η is the Spitzer resistivity, λ is the Taylor eigenvalue ($\nabla\times\boldsymbol{B} = \lambda\boldsymbol{B}$ in the force-free spheromak) and $1/\lambda = a_{CT}/4.493$ (a_{CT}: the radius of CT sphere) in the spherical geometry [11]. Typical electron temperature of a spheromak is a few tenth of eV [24, 25] and this gives η of the order of 10^{-5} $\Omega\cdot$m. Accordingly, τ_{CT} is 5×10^{-5} sec in the case of a_{CT} = 0.1 m, for example. Because α is determined by the CT radius that cannot exceed the main plasma radius, it is efficient to heat up the CT and increase the electron temperature to extend τ_{CT}. The simplest heating scheme that requires no external devices is the adiabatic compression. Although CT compression has been already adopted in recent CT injectors, only an increase of the CT density has been highlighted. To carry out the adiabatic compression to increase the temperature, it is necessary to keep proper relations between the CT compression time τ_{comp} and other time-constants such as collision time, energy confinement time, and the time of Alfvén wave transmission across the CT radius τ_A [26-29]. For example, $\tau_A \ll \tau_{comp}$ is required to compress the CT self-similarly without generating shock waves. Although the typical CT injectors have been equipped with the compression cones after the straight co-axial electrodes, the condition $\tau_A \ll \tau_{comp}$ has not been achieved due to insufficient length of the cones. In this paper, a conical accelerator is proposed to extend τ_{comp} as long as the CT acceleration time τ_{acc}. Changes in CT parameters such as the magnetic field strength, the temperature, and the density *etc.* before and after the compression are calculated assuming the adiabatic condition.

As mentioned above, one can obtain the high acceleration efficiency when the ratio R_{out}/R_{in} is large enough. Large R_{out}/R_{in} means relatively small R_{in} that results in the comparatively strong magnetic field around the inner-electrode. If the acceleration current I_{acc} is extremely large, the current blows out CT and normal acceleration is hardly achieved. Experimentally, the threshold to avoid this "blowby" phenomenon is given by $B_{CT} > B_{acc}$, where B_{CT} is CT magnetic field and B_{acc} is the magnetic field generated by I_{acc} (refs. 5-7). Therefore, B_{CT}, which is mainly determined by the bias magnetic field, should be larger than B_{acc}, which is large when R_{in} is small. On the other hand, smaller bias magnetic field is favorable because that requires the less formation current, which should be large enough to push the current sheet out of the formation electrode, and mitigates the capacitor banks for CT formation. The minimum bias magnetic field to avoid the blowby phenomenon is derived through the optimization of the acceleration part. The design of the CT formation part is determined using this bias magnetic field.

CT injection experiment on LHD is intended for the active particle control as well as the center fueling. This will be the first CT application on the helical plasma. In the helical magnetic field, the CT traces the three-dimensional trajectory, which can be used to inject the CT momentum effectively [19]. A design of CT injector for LHD is given in this study. One of the main goals of this design is to achieve the highest acceleration efficiency while avoiding the blowby phenomenon. Device parameters of the injector including its fueling ability and the technological conditions that limits the size of electrodes are given in section 2. The point-model that describes the motion of CT in the co-axial electrode is introduced in section 3, and the acceleration efficiencies calculated by the point-model are compared with that obtained from the analytic model. Compression parameters of the conical accelerator suggested in this introduction are estimated assuming the adiabatic condition and given in section 4. The optimized acceleration electrode design and the resultant condition for CT formation such as the minimum bias magnetic field are also given. The experimental scenario to carry out the CT injection on LHD is discussed in section 5, together with the injector design that has been already assembled. Summary is given in section 6.

2. Design parameters of CT injector for LHD

LHD is the largest super-conducting fusion machine with the heliotron configuration. The major radius of the torus is 3.9 m and the magnetic field strength on the plasma center is 3 T. The field period around the torus is 10, and the pole number of helical coil winding is two. The plasma minor radius is changeable from 0.5 m to 0.65 m, by controlling the ratios of coil currents in helical coils and poloidal coils. In the standard configuration, the major radius of the LHD plasma is 3.75 m. Details of LHD and its program are presented in refs. 22 and 23.

The design parameters of the CT injector for LHD are summarized in Table I. Fuel plasmoid with weigh of about 0.1 mg, which corresponds to about 10 % of LHD plasma particles, will be injected. Although this CT mass can be controlled by changing the gas pressure in the formation part before the discharge or changing the working gas to heavier one such as He, the weight of 0.1 mg is assumed almost throughout this study. Mass dependence of the acceleration efficiency is discussed in section 5. Target velocity is more than 500 km/s and CT kinetic energy over 15 kJ should be achieved to carry out the CT injection into 3 T LHD plasmas.

Nine parameters listed in Table II are used to describe the CT acceleration electrodes. This acceleration part has conical shape as shown in Fig. 1. Three parameters (R_{in1}, C_{acc}, and E_{acc}) are mainly discussed in this paper while other six parameters are determined as below. The outer electrode radius at the exit of acceleration part R_{out2} determines the radius of an injected CT. Small CT is favorable because the perturbation caused by CT injection should be smaller and localized. In our case, R_{out2} (= 0.07 m) is determined to be about one tenth of the typical averaged minor radius of LHD. Total amount of particles N_{CT} and the CT lifetime τ_{CT} are related to the size of CT at the entrance of the acceleration part that is defined as R_{out1}. Although large R_{out1} is favorable to increase both of N_{CT} and τ_{CT}, extremely large R_{out1} results in an unfavorably large size CT injector. In the present case, R_{out1} (= 0.17 m) is more than twice larger than R_{out2}, while it allows the use of the standard flanges (ICF406, for instance). Aspect ratio of CT at the exit of the acceleration part A_2 is determined by R_{out2} and R_{in2} as $A_2 \equiv R_2/a_2$ ($a_2 \equiv (R_{out2}-R_{in2})/2$, and $R_2 \equiv R_{in2}+a_2$). Because the aspect ratio just after the exit of the acceleration part is one, A_2 should be as small as possible to avoid the large modification of CT shape. Therefore, R_{in2} = 0.02 m is adopted. Note that extremely small R_{in2} should not be chosen because the Joule heating by the acceleration current might melt down the electrode The external inductance L_{ext} and the circuit resistance R_c should be as small as possible to maximize the acceleration efficiency ε as will be discussed in the next section. The length of the acceleration part l should be long enough to have large L that results in large ε and to realize slow and self-similar compression. Extremely large l might increase the impurity level contained in a CT and enlarge the size of CT injector, on the other hand. In this study, l = 3.2 m is adopted. Other cases with l = 0 8m and l = 1.6m are also examined in sections 4 and 5. As will be mentioned there, l = 0.8m is adopted in our first CT injector named SPICA mk. I.

Table I. Design parameters for SPICA mk. I.

CT volume, V_{CT} (m^3)	1×10^{-3} to 5×10^{-3}
CT electron density, n_e (m^{-3})	1×10^{21} to 2×10^{22}
CT mass, m_{CT} (μ g)	2 to 170
Particle inventory, N_{CT}	1×10^{19} to 1×10^{20}
CT magnetic field, B_{CT} (T)	1 0 to 3 0
CT initial velocity, v_0 (km/s)	200 to 500
CT kinetic energy E_{CT} (kJ)	> 15
CT electron temperature T_e (eV)	10 to 100
Working gas	H_2 He, Ne etc

Table II Main parameters used to design the acceleration electrode.

Inner radius at the entrance, R_{in1} (m)	*to be optimized.*
Outer radius at the entrance, R_{out1} (m)	0 17
Inner radius at the exit, R_{in2} (m)	0 02
Outer radius at the exit, R_{out2} (m)	0 07
Electrode length, l (m)	3 2 (/ 1 6 / 0 8)
Resistance of the circuit, R_c (Ω)	< 0 03
Capacitance of the bank, C_{acc} (F)	*to be optimized.*
Stored energy of the bank, E_{acc} (J)	*to be optimized.*
External inductance, L_{ext} (H)	< 5×10^{-7}

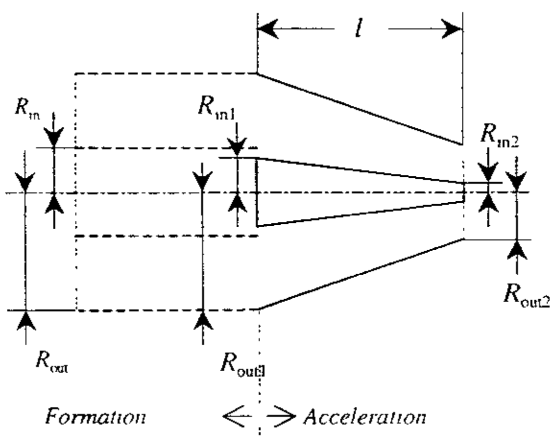

Fig. 1 Geometry of a conical accelerator. CT enters from the left-hand-side and exits to the right-hand-side. CT formation electrode is drawn by broken lines

3. Point-model of acceleration and acceleration efficiency ε

One-dimensional motion of a CT in the acceleration electrode is described by the point-model introduced by Hammer *et al.* in ref. 7. Although their model assumes no resistivity in the acceleration circuit, it agrees well with experimental results. The point model with consideration of circuit resistivity R_c consists of three equations below,

$$L_t = L_{ext} + L, \qquad (1)$$

$$\frac{d^2 I_{acc} L_t}{dt^2} + R_c \frac{d I_{acc}}{dt} + \frac{I_{acc}}{C_{acc}} = 0, \qquad (2)$$

$$m_{CT} \frac{d^2 x}{dt^2} = \frac{1}{2} L' I_{acc}^{\ 2} - F_{drag}, \qquad (3)$$

where $L = \int_0^l L' dx$ ($L' = \mu_0/(2\pi)\ln(R_{out}(x)/R_{in}(x))$, and $0 \leqq x \leqq l$) is the inductance of the co-axial electrode, L_t is the total inductance of the acceleration circuit, I_{acc} is the circuit current, C_{acc} is the capacitance of the acceleration bank, m_{CT} is the CT mass, and F_{drag} is the drag force. In this study, $F_{drag} = 0$ is assumed since it is negligibly small as in ref. 7. Time dependence of R_c is neglected in Eq. (2), although it consists of time-dependent component such as plasma resistivity and electrode resistivity that depends on the CT position in the electrode. Since the plasma resistivity of the order of 10^{-4} Ω is negligible in our case, this approximation is valid as long as the electrode resistivity (of the order of 10^{-3} Ω) is smaller enough than the other circuit resistivity. In a general straight co-axial electrode, the inner-electrode radius R_{in} and the outer-electrode radius R_{out} are constant and $L_t = L_{ext} + L'x$. In the case of the conical accelerator, $R_{in}(x) = R_{in1} + (R_{in2} - R_{in1}) \cdot x/l$ and $R_{out}(x) = R_{out1} + (R_{out2} - R_{out1}) \cdot x/l$. Using the expressions in Eqs (1) - (3), the CT kinetic energy E_{CT} is given by $m_{CT}(dx/dt)^2/2$ and the acceleration bank energy E_{acc} is given by $C_{acc}V_{acc}^{\ 2}/2$, where V_{acc} is the bank voltage.

The fourth-order Runge-Kutta method is used to solve Eqs. (1) - (3). Figure 2 shows the calculation results for a straight co-axial electrode with $R_{out}/R_{in} = 2$ and $l = 3.2$m. Three different cases are calculated while changing C_{acc} and R_c. As seen in the differences between Fig. 2(a) and Fig. 2(b), CT obtains less kinetic energy when R_c is not zero. The energy loss due to R_c occurs mainly in the current increasing phase (before $t \sim 5$ μsec) and then E_{CT} gradually increases. In other words, the transfer of the energy from the acceleration bank (E_{acc}) to the CT (E_{CT}) occurs mainly after the current peaks. Therefore the current peak should be obtained before the CT exits the acceleration electrode and smaller C_{acc} should be used because the oscillation frequency

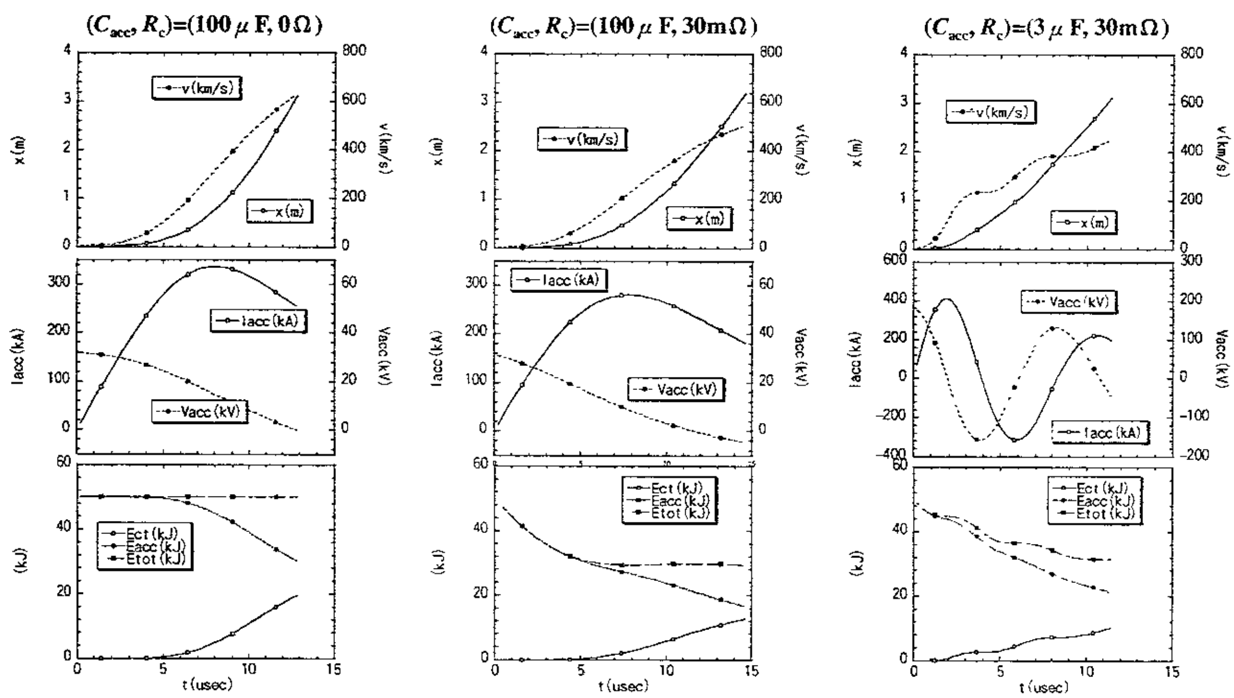

Fig. 2 Calculated waveforms of CT position x and CT velocity v (top), acceleration current I_{acc} and acceleration voltage V_{acc} (middle), CT kinetic energy E_{CT}, circuit energy E_{acc} and the total energy $E_{tot} = E_{CT} + E_{acc}$ (bottom). Assumed C_{acc} and R_c are indicated on the top of each column.

of this LCR circuit is proportional to $1/C_{acc}^{1/2}$. Note that extremely small C_{acc} results in the large acceleration bank voltage V_{acc}, which might be not realistic, to obtain the same bank energy as in moderate C_{acc} case. Moreover, too small C_{acc} results in the oscillation of the current as shown in Fig. 2(c) and E_{CT} is not necessarily larger than that obtained with moderate C_{acc} (as in Fig. 2(b)). The voltage reversal should be avoided since it is harmful to the circuit, and especially to the high-voltage trigger system that uses ignitrons. The current damping condition $R/(2L) > 1/\sqrt{LC}$ should be fulfilled for this requirement.

The acceleration efficiency ε as a function of C_{acc} is calculated using different values of R_c and E_{acc}, where the other parameters such as L_{ext} and the electrode shape L' are fixed. The results are shown in Fig. 3. When $R_c = 0\ \Omega$, the maximum of acceleration efficiency ε_{max} does not depend on E_{acc}. Finite R_c reduces ε_{max} and the reduction rate is larger when E_{acc} is smaller. Although R_c degrades ε_{max}, the optimum C_{acc} that gives ε_{max} is not affected by R_c. Coulomb numbers of the bank $Q = C_{acc}V_{acc}$ calculated for the optimum cases are also constant, and $Q \sim 2.4$ C in the case shown in Fig. 3. These observations mean that once an electrode is designed and assembled, the acceleration efficiency that can be achieved with the electrode is already determined, and the optimum C_{acc} for each E_{acc} should be adopted to attain the largest ε.

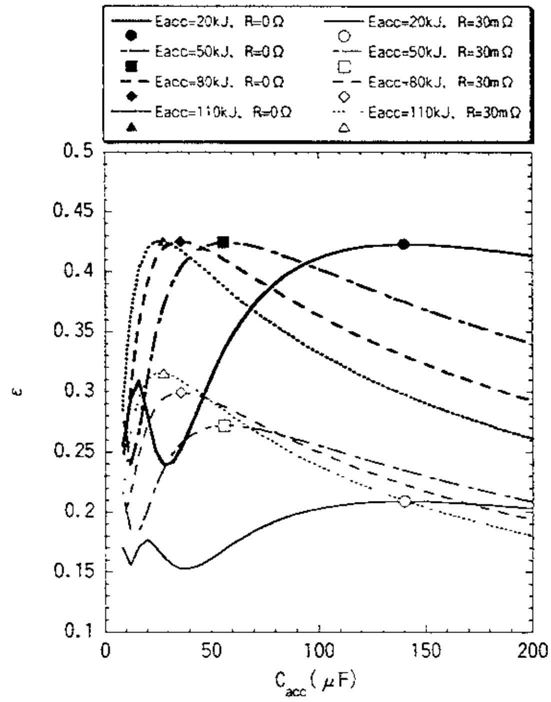

Fig. 3 Acceleration efficiency as a function of C_{acc}. Straight co-axial electrode geometry with l = 3.2 m, R_{out}/R_{in} = 2, m_{CT} = 0.1 mg, F_{drag} = 0 N, v_0 = 5 km/s and L_{ext} = 0.5 μH are used in this calculation, where E_{acc} and R_c are scanned as indicated on the top of the figure. The maximum efficiencies are marked with symbols.

It is possible to show that ε_{max} does not depend on E_{acc} but on the ratio of the electrode inductance to the external inductance. Let us consider a general LCR circuit without external power supplies. The circuit equation is given by

$$L\frac{dI}{dt} + RI + \frac{Q}{C} = 0. \quad (4)$$

Zero-resistivity condition gives the harmonic oscillation with the eigenfrequency $\omega_0 = 1/\sqrt{LC}$ as the solution. When the resistivity is finite, the solution is the damped oscillation where the amplitude decreases with time as $\exp(-\gamma t)$ ($\gamma = R/(2L)$). In the present case, dL/dt is not zero and the circuit equation is given by

$$\frac{d(LI)}{dt} + RI + \frac{Q}{C} = L\frac{dI}{dt} + \left(\frac{dL}{dt} + R\right)I + \frac{Q}{C} = 0, \quad (5)$$

instead of Eq. (4). Note that Eq. (2) is obtained by differentiating Eq. (5) with t. It can be seen in Eq. (5) that dL/dt plays the same role as R, and therefore gives the damped oscillation as the solution even if $R = 0$. Here let L and dL/dt be fixed to evaluate the order of damping time constant γ. These are not constant in practical situation since L is the function of the current sheet position x in the electrode and dL/dt depends on the velocity $v = dx/dt$. Using fixed parameters, *i.e.*, $L^* = L_{ext}+L/2$ and $dL^*/dt = (L_t - L_{ext})/\tau_{acc} = L/\tau_{acc}$, the approximated damping time constant γ^* for zero-resistivity is given by

$$\gamma^* = \frac{dL^*/dt}{2L^*} = \frac{L}{2L_{ext}+L}\frac{1}{\tau_{acc}} = \frac{m}{2+m}\frac{1}{\tau_{acc}}, \quad (6)$$

where $m \equiv L/L_{ext}$. The energy of the circuit decreases as $(\exp(-\gamma^* t))^2$ and the lost energy should be equal to the CT kinetic energy to fulfill the energy conservation law. Therefore, the approximated CT kinetic energy E_{CT}^{*} is given by

$$E_{CT}^{*} = E_{acc}(1-\exp(-2\gamma^{*}t)). \quad (7)$$

The ratio of E_{CT}^{*} with $t = \tau_{acc}$ to the bank energy E_{acc} gives the approximated efficiency ε^{*};

$$\varepsilon^{*} = \frac{E_{CT}^{*}}{E_{acc}} = 1-\exp(-2\gamma^{*}\tau_{acc}) = 1-\exp\left(-\frac{m}{2+m}\right). \quad (8)$$

This function is shown in Fig. 4 with a solid line. The maximum efficiencies calculated using the fourth-order Runge-Kutta method with different parameters are also plotted in the figure. It can be seen that ε^{*} approximates ε_{max} well. The key to obtain large ε_{max} lies in m. Therefore, large L and/or small L_{ext} are the indispensable conditions for a high performance CT injector.

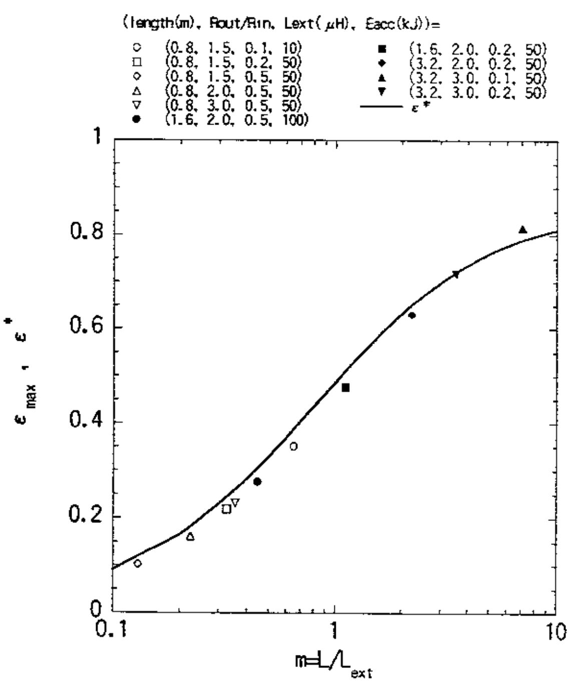

Fig. 4 The maximum efficiencies calculated for various parameter sets and the approximated efficiency ε^{*} (solid line). Straight co-axial electrode geometry, $m_{CT} = 0.1$ mg, $F_{drag} = 0$ N, $v_0 = 5$ km/s are fixed throughout the optimization.

4. Adiabatic compression using conical accelerator and formation electrode design

As mentioned in the introduction, the adiabatic compression heating using a conical accelerator is effective to increase τ_{CT}. The adiabatic conditions τ_{ee}, τ_{ii}, $\tau_{A} \ll \tau_{comp} \ll \tau_{E}$, τ_{CT}, should be fulfilled to realize compression heating, where τ_{ee} and τ_{ii} are electron-electron and ion-ion collision time, respectively, and τ_{E} is energy confinement time. The relations between these time constants, which are calculated using typical parameters described in Table I, are depicted in Fig. 5. Although τ_{E} is unknown, τ_{comp} should be sufficiently larger than τ_{A}, because $\tau_{A} \ll \tau_{comp}$ is needed to realize the self-similar compression. The largest τ_{comp} is obtained when the length of the compression cone and that of the acceleration electrode are the same and $\tau_{comp} = \tau_{acc}$ as is the case of the conical accelerator. Here let us calculate the compression parameters assuming the adiabatic condition. Each of parameters of general toroidal plasma depends on the CT minor radius a and the CT major radius R as listed in Table III. The relations in Table III are obtained assuming the adiabatic condition $T \cdot n^{1-5/3} = constant$, and $B_p \sim B_t$.

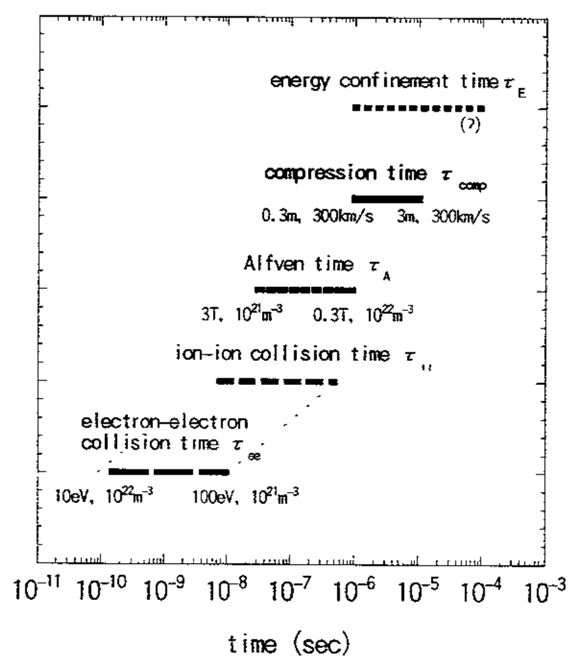

Fig. 5 Characteristic time scales of typical CTs and accelerators.

Table III. Adiabaticaly compressed parameters as functions of the minor radius a and the major radius R of toroidal plasma. The adiabatic condition $T \cdot n^{1-5/3}$ = *constant* and $B_t \sim B_p$ are assumed.

Toroidal field strength, B_t	$\propto a^{-2}$
Poloidal field strength, B_p	$\propto a^{-1} R^{-1}$
Plasma volume, V	$\propto a^2 R$
Plasma density, n	$\propto a^{-2} R^{-1}$
Plasma temperature, T	$\propto a^{-4/3} R^{-2/3}$
Plasma pressure, p	$\propto a^{-10/3} R^{-5/3}$
Magnetic pressure, $\propto B^2$	$\propto a^{-2}(a^{-2} + R^{-2})$
Plasma beta, β	$\propto a^{-4/3} R^{-5/3} (a^{-2}+R^{-2})^{-1}$

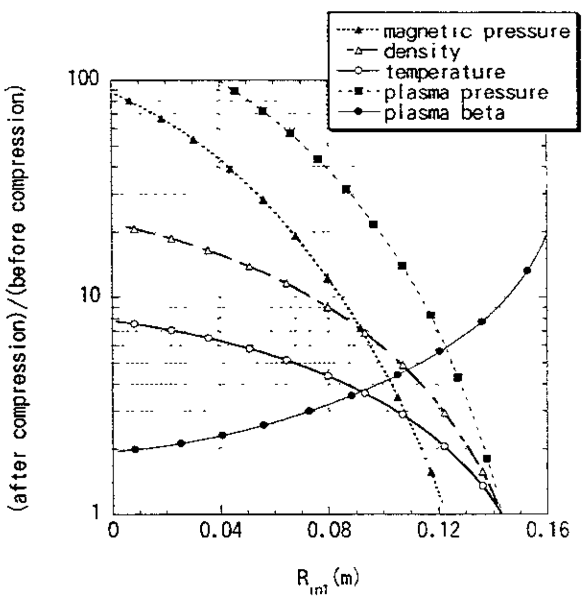

Fig. 6 Compression parameters of adiabaticaly compressed toroidal plasmas, where R_{out1} = 0.17 m, R_{out2} = 0.07 m and R_{in2} = 0.02 m are fixed. Adiabatic condition of $T \cdot n^{1-5/3}$ = *constant* and $B_p \sim B_t$ are assumed.

The increment factors are calculated and shown in Fig. 6. The temperature (density) increases more than four (eight) times after the compression when R_{in1} is smaller than the half of R_{out1} (= 0.17 m). The large plasma pressure might cause some pressure driven instability on the other hand. In the present case, the pressure increases more than thirty times when $R_{in1} < R_{out1}/2$. However, the increase in the magnetic field pressure helps to suppress the increase of plasma beta lower than a factor of three even in that case. The CT magnetic field B_{CT} should be larger than the magnetic field B_{acc} generated by the acceleration current. Otherwise, the CT might be deformed and normal acceleration will hardly be realized [5-7]. This is called "blowby" effect. In the case of a conical accelerator, B_{CT} increases during acceleration when the compression is effective. The least magnetic field strength at the entrance of conical accelerator, B_{01}, should be determined using the condition that B_{CT} is always larger than B_{acc} during the acceleration phase.

To optimize the electrode design, C_{acc} is scanned to obtain the largest ε for each R_{in1} where l = 3.2 m, R_{out1} = 0.17 m, R_{out2} = 0.07 m, R_{in2} = 0.02 m, and E_{acc} = 75 kJ are fixed. Three different cases of (L_{ext}, R_c) = (0.2 μH, 0 Ω), (0.5 μH, 0 Ω), and (0.5 μH, 0.03 Ω) are calculated and the optimum values of C_{acc}, V_{acc}, and ε are plotted as functions of R_{in1} in Fig. 7. The least B_{01} in each case are also shown in the figure. The maximum ε increases as R_{in1} decreases, and in this sense, R_{in1} should be as small as possible. On the other hand, the optimum V_{acc} is large when R_{in1} is small. One can determine the optimum R_{in1} using Fig. 7. First, the target CT kinetic energy and ε determine the bank energy. In our case, $E_{CT} \geqq$ 15 kJ should be achieved and more than 38 % of ε is expected for $R_{in1} \leqq$ 0.07 m. Therefore, E_{acc} = 40 kJ is enough to obtain the target E_{CT}. Note that ε is not affected by E_{acc} when R_c = 0, as is already mentioned in section 2. Using the fact that $Q = C_{acc} V_{acc}$ is also unchanged by E_{acc} (see section 2), the relation $E_{acc} \propto V_{acc}$ is obtained. Thus V_{acc} in Fig. 7 can be reduced to about half because E_{acc} = 75 kJ is used to obtain the figure. When V_{acc} is limited to 40 kV, for instance, R_{in1} = 0.07 m can be chosen with E_{acc} = 42.4 kJ, and the achievable E_{CT} is 14.5 kJ in that case (L_{ext} = 0.5 μH and R_c = 0.03 Ω). One should note that the maximum ε slightly decreases with E_{acc} when R_c is not negligible (see Fig. 3). The least B_{01} for R_{in1} = 0.07 m is 0.62 T in Fig. 7. This can be also reduced if small E_{acc} is adopted. In the case of E_{acc} = 42.4 kJ, B_{01} is calculated to be 0.46 T.

The next step is to design the formation electrode. The inner radius of the formation electrode R_{in} should be slightly larger than that of the accelerator electrode R_{in1}, to isolate electrically from each other (see Fig. 1). Let this gap be 0.02 m, then R_{in} should be 0.09 m. The outer radius of the formation electrode R_{out} is

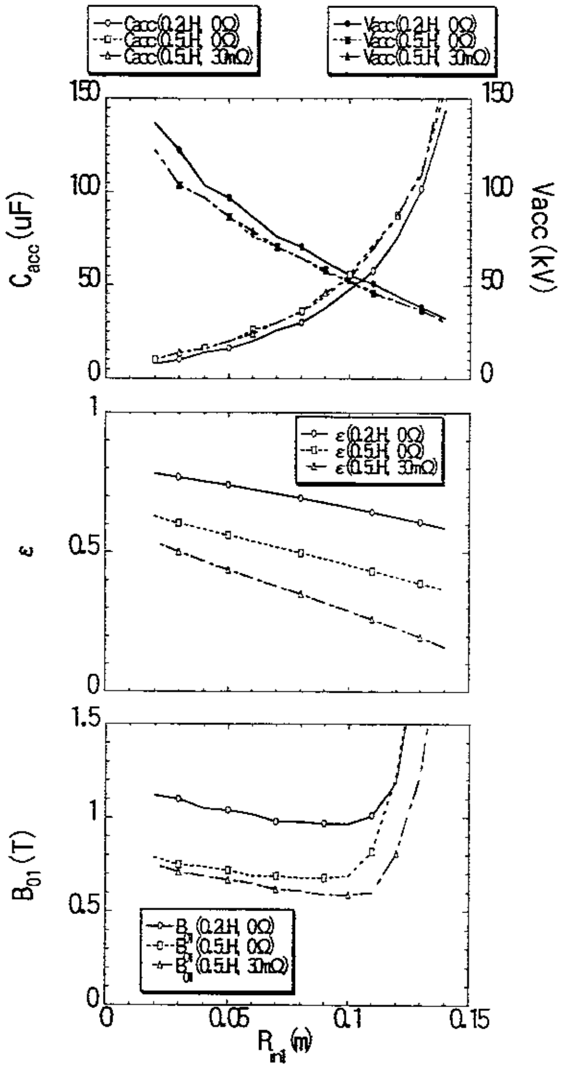

Fig. 7 Optimized parameters in three different cases. The optimum C_{acc} and V_{acc} (top), the acceleration efficiency ε (middle), and the least magnetic field strength at the entrance of the acceleration part B_{01} (bottom) are shown as functions of R_{in1}. Assumed R_c and L_{ext} are indicated in each plot. The other parameters such as E_{acc} = 75 kJ, l = 3.2 m, R_{out1} = 0.17 m, R_{out2} = 0.07 m, R_{in2} = 0.02 m , m_{CT} = 0.1 mg, F_{drag} = 0 N, v_0 = 1 m/s are fixed throughout this optimization.

defined to be the same as that of the accelerator, thus $R_{out} = R_{out1}$ = 0.17 m. The gap distance Δd between the inner- and the outer-electrode is 0.08 m in this case. The CT magnetic field B_{CT} should be the same as or larger than B_{01} calculated in Fig.

7. Another important parameter to be determined is the formation current I_{form}. There is a relation, which should be fulfilled to form a CT, between Δd and I_{form} as

$$I_{form} > \frac{\pi}{\Delta d}\frac{\Phi_{bias}}{\mu_0}, \tag{9}$$

where Φ_{bias} is the bias magnetic flux passing through the inner electrode. This means that the magnetic pressure generated by I_{form} should be larger than the drag force due to the magnetic pressure of the bias magnetic field. This equation gives the least I_{form} and has been confirmed by experimental observations (refs. 30-32). The CT magnetic field B_{CT} is derived from B_{form} (toroidal component) and B_{bias} (poloidal component) defined as below,

$$B_{form} = \frac{\mu_0 I_{form}}{2\pi(R_{out}+R_{in})/2}, \tag{10}$$

$$B_{bias} = \frac{\Phi_{bias}}{\pi R_{in}^2}. \tag{11}$$

In a force-free magnetic configuration such as spheromak, the magnetic helicity (which is proportional to the multiple of toroidal- and poloidal-magnetic fluxes) is conserved [30, 33]. Let us define the helicity $K = 2\Phi_1\Phi_2$, where $\Phi_1 = B_{form}S_1$ and $\Phi_2 = B_{bias}S_2$. After the magnetic reconnection, the averaged strengths of the toroidal-magnetic fields $B_t = \Phi_1'/S_1'$ and poloidal-magnetic fields $B_p = \Phi_2'/S_2'$ are almost the same in a spheromak and $2\Phi_1'\Phi_2' = K = 2B_{form}B_{bias}\cdot S_1S_2$ since the helicity is conserved. Therefore, $B_{CT}^2 \sim B_t\cdot B_p = \Phi_1'\Phi_2'/(S_1'\ S_2') = B_{form}B_{bias}$ when $S_1=S_1'$ and $S_2=S_2'$, or,

$$B_{CT} = \sqrt{B_{form}\cdot B_{bias}}. \tag{12}$$

Let I_{form} be equal to the right-hand-side of Eq. (9), to obtain the relations below,

$$I_{form} = \alpha B_{CT}, \tag{13}$$

$$\alpha = \frac{\pi R_{in}}{\mu_0}\sqrt{\frac{\pi(R_{out}+R_{in})}{R_{out}-R_{in}}}. \tag{14}$$

The factor α is plotted in Fig. 8 as a function of R_{in}, where R_{out} = 0.17 m is fixed. The minimum I_{form} is derived using Eq. (13) and substituting B_{01}

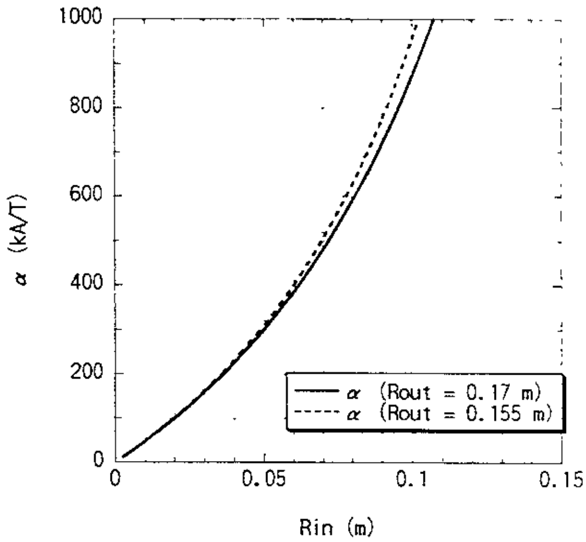

Fig. 8 The least formation current factor α as a function of R_{in} ($I_{form} = \alpha B_{CT}$). Solid line shows α in the case of R_{out} = 0.17 m, which is the same as the radius of acceleration outer-electrode at the entrance R_{out1}, and dashed line is that of R_{out} = 0.155 m, which is the case of SPICA mk. I as shown in Fig. 9.

for B_{CT}. From Eq (14), α is calculated to be 719.0 kA/T. If B_{0l} of 0.46 T is needed, 719.0× 0 46 =330.7 kA of I_{form} should be supplied at least

As will be mentioned in the next section, three types of conical accelerator are considered The difference between them is the length of the acceleration electrode l. Although the long electrode of l = 3.2 m has the merit of large efficiency, both the construction cost and the technological difficulty increase. Therefore, other two cases with l = 0.8 m and l = 1.6 m are also optimized according to the process already mentioned above for l = 3.2 m. The optimized parameters are listed in Table IV. The available voltage for V_{acc} is limited to 40 kV or 20 kV in this series of optimization. The moderate length electrode of l = 1.6 m is still usable since the achievable E_{CT} is over 7 kJ which is enough for CT injection into 1.5 T LHD magnetic field The shortest length electrode of l = 0.8 m can achieve only 3.4 kJ of E_{CT} in the optimum condition, and it is also difficult to fulfill the adiabatic condition because of the small τ_{acc} (= τ_{comp}).

Table IV. The optimized parameters for different acceleration electrode lengths and voltage limits.

Device Name	SPICA mk. I	SPICA mk. I	SPICA mk. II	SPICA mk. II	SPICA mk III	SPICA mk. III
Assumed parameters						
l (m)	0.8	0.8	1.6	1.6	3.2	3 2
R_{in1} (m)	0.07	0 07	0.07	0.07	0.07	0 07
R_{out1} (m)	0.17	0 17	0.17	0.17	0.17	0 17
R_{in2} (m)	0.02	0.02	0.02	0.02	0.02	0.02
R_{out2} (m)	0.07	0.07	0.07	0.07	0 07	0.07
L (H)	1.6×10^{-7}	1.6×10^{-7}	$3\ 2\times10^{-7}$	3.2×10^{-7}	$6\ 4\times10^{-7}$	6.4×10^{-7}
L_{ext} (H)	5.0×10^{-7}	5.0×10^{-7}	5.0×10^{-7}	5.0×10^{-7}	$5\ 0\times10^{-7}$	5.0×10^{-7}
R_c (Ω)	$3\ 0\times10^{-2}$	3.0×10^{-2}	$3\ 0\times10^{-2}$	3.0×10^{-2}	$3\ 0\times10^{-2}$	3.0×10^{-2}
m_{CT} (kg)	1.0×10^{-7}	1.0×10^{-7}	1.0×10^{-7}	1.0×10^{-7}	$1\ 0\times10^{-7}$	$1\ 0\times10^{-7}$
v_0 (m/s)	1 0	1.0	1 0	1.0	1.0	1 0
V_{acc} (V)	$2\ 0\times10^{4}$	4.0×10^{4}	$2\ 0\times10^{4}$	4.0×10^{4}	$2\ 0\times10^{4}$	$4\ 0\times10^{4}$
Optimized parameters						
E_{acc} (J)	1.10×10^{4}	2.19×10^{4}	1.55×10^{4}	3.10×10^{4}	2.12×10^{4}	4.24×10^{4}
C_{acc} (F)	5.48×10^{-5}	2.74×10^{-5}	7.75×10^{-5}	3.87×10^{-5}	1.06×10^{-4}	$5\ 30\times10^{-5}$
I_{acc} (A)	1.58×10^{5}	2.35×10^{5}	1.75×10^{5}	2.61×10^{5}	$1\ 89\times10^{5}$	$2\ 82\times10^{5}$
B_{0l} (T)	0.25	0 37	0 28	0.41	0.31	0 46
I_{form} (A)	$1\ 80\times10^{2}$	2.66×10^{2}	2.01×10^{2}	2.95×10^{2}	2.23×10^{2}	$3\ 31\times10^{2}$
τ_{acc} (s)	$1\ 17\times10^{-5}$	8.03×10^{-6}	$1\ 47\times10^{-5}$	9.98×10^{-6}	1.90×10^{-5}	$1\ 28\times10^{-5}$
ϵ	0.135	0 157	0 207	0.244	0 286	0 342
E_{CT} (J)	1.49×10^{3}	3.43×10^{3}	3.20×10^{3}	7.56×10^{3}	6.07×10^{3}	1.45×10^{4}

5. Experimental scenario to inject a CT into LHD

The goal of CT injection is to increase the core density of LHD plasmas. As is mentioned in the introduction, more than 15 kJ of E_{CT} is necessary to carry out the effective CT injection into LHD plasmas confined in 3 T magnetic field. Considering the CT injection into 1.5 T magnetic field, the least E_{CT} is reduced to about 4 kJ. Although 14.5 kJ of E_{CT} can be achieved with the conical accelerator of length 3.2 m as mentioned in the sections above, the difficulty in making and handling of a long electrode and its construction cost increase. Therefore, short conical accelerator of length 0.8 m is adopted in the first step. The scenario to achieve our goal is like this;

step 1) develop the formation electrode and 0.8 m conical accelerator, install the formation banks and carry out CT formation experiments,

step 2) install the acceleration banks and carry out CT acceleration experiments,

step 3) develop 1.6 m conical accelerator and carry out CT acceleration experiments,

step 4) develop 3.2 m conical accelerator and carry out CT acceleration experiments.

In any step where E_{CT} = 15 kJ is achieved, the scenario goes to the final step that includes the CT injection experiments on LHD. In the case of LHD, the distance from the injection port to the core of LHD plasma is as long as 4 m. The injected CT should fly a few meters after the acceleration electrode without any supports by conducting shells, and suffering the stray magnetic field of LHD. The target transfer distance is set to 5 m. Since such a long CT transfer has not been realized, how to support the CT from decaying or wandering is the major subject to be researched throughout this scenario. Reduction in the impurity level is another important subject. Baking technique and glow-discharge-cleaning are prepared to remove the impurities on the electrode surfaces. These wall conditioning will be carried out from the beginning of (and throughout) the experiments.

The CT injector named SPICA mk. I (SPheromak Injector using Conical Accelerator) was successfully assembled on March 1999. The design of this device is based on the results of this study. Schematic view and the photograph of SPICA mk. I are shown in Fig. 9. SPICA is equipped with some characteristic parts that

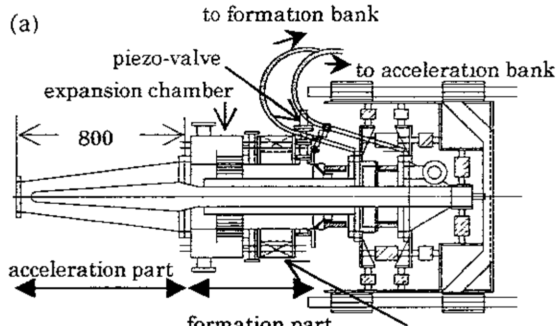

(b)

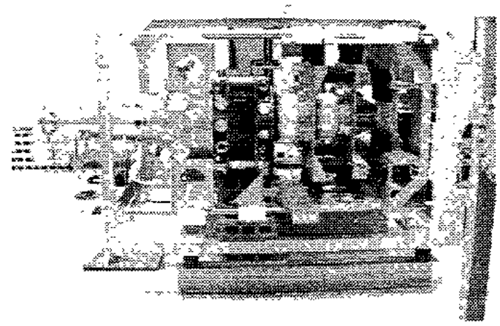

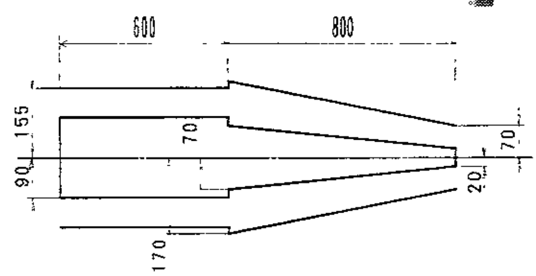

(c) Geometry of one-stage operation with two-stage electrode.

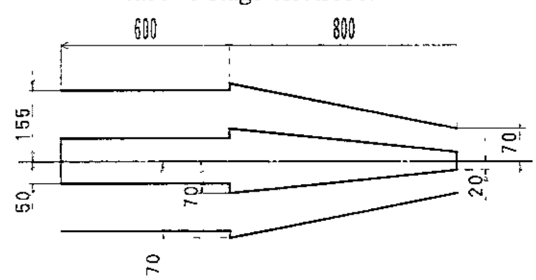

(d) Geometry of one-stage electrode.

Fig. 9 (a) Schematic of SPICA mk. I and (b) the photograph from the same view point. Electrode geometry used to examine the one-stage operation with electrically connected two inner-electrodes is shown in (c), and the geometry of one-stage electrode after removal of the formation inner-electrode is depicted in (d).

cannot be seen on the other CT injectors, such as the conical electrode, the expansion chamber for strong differential pumping, and fast piezo-valves for gas injection into the formation part. The expansion chamber is necessary to pump out the neutral gas that is not ionized in the injector. The inflow of neutral gas into the main plasma is not favorable because this makes it difficult to see the fueling effect only by a CT. Although this chamber is equipped with a turbo molecular pump of pumping rate 1,000 l/s, inside of this chamber will be Ti coated to obtain the larger pumping rate of over 20,000 l/s. Another turbo molecular pump of pumping rate 200 l/s is also equipped on the acceleration electrode flange to pump the volume between the two inner-electrodes of formation and acceleration. Use of fast piezo-valves, of which the time for full open to full close (or vice versa) is less than 10^{-3} s, are also different from the other CT injectors which adopt the solenoid-valves in general. Stable flow rate and less mechanical shocks are the merits of the piezo-valves compared to the solenoid-valves. Hot silicone oil of temperature ~140 ℃ is circulated inside the acceleration inner-electrode to bake out the water on its surface. The outer-electrode is also baked using ribbon-heaters. The biasing coil is set around the outer electrode of formation part. This coil consists of copper conductor of 4 mm×9 mm cross-section that is wound 201 turns.

According to the results of section 4, SPICA mk.I can achieve only small ε (= 15.7 %) since the length is short and thus the inductance of acceleration part is small compared with L_{ext}. Reduction in L_{ext} or R_c is effective to attain larger ε although it is technological issue and might be difficult. The mass of CT affects ε as will be mentioned later in this section, therefore larger ε can be also obtained by optimizing m_{CT}. The key parameter for large ε is the electrode inductance L. To make a full use of this feature, a common power supply to acceleration and formation, *i.e.*, connection of two inner electrodes is considered as an option in SPICA mk. I. In this case, only one power supply forms and accelerates the CT. Although the optimization in sections above implicitly assumes two power supplies for formation and acceleration, it is still possible to apply the optimization process to this "one-stage operation". Reduction in the number of power supply results in the large cost reduction at the same time. The difficulty in this operation is mainly in the CT formation part. The least B_{CT} to avoid blowby phenomenon and resultant I_{form} can be determined independently of E_{acc} in the section 4. In the case of one-stage operation, I_{form} is a function of E_{acc}, which plays two roles of formation and acceleration. Therefore once the electrode geometry and E_{acc} are determined, the condition to avoid the blowby phenomenon can be calculated. In the case of SPICA mk I, ε, $E_{CT} = \varepsilon E_{acc}$, and $I_{max}/(\alpha B_{01})$ are plotted as functions of E_{acc} in Fig. 10. In this series of calculation, $C_{acc} = 400\,\mu$F ($100\,\mu$F) is fixed to limit $V_{acc} \leqq 20$ kV (40 kV) with $E_{acc} \leqq 80$ kJ. The electrode geometry used in this

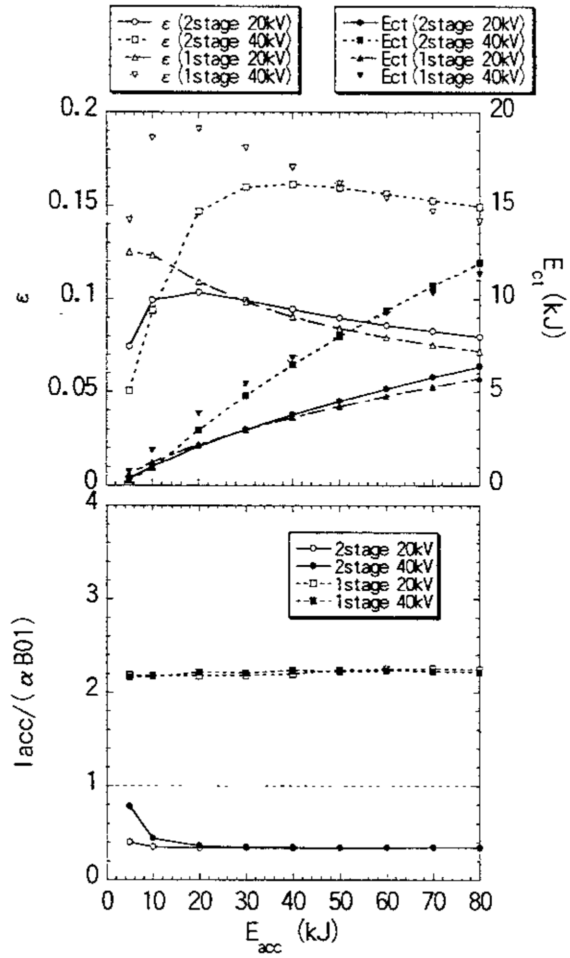

Fig. 10 Acceleration efficiency and CT kinetic energy within the limitation of acceleration voltage (top figure). The bottom figure is the ratio of I_{acc} to the least formation current αB_{01}, which should be larger than one to avoid the blowby phenomenon. The case of one-stage operation with two-stage electrode (Fig. 9(c)) and that of one-stage electrode (Fig. 9(d)) are calculated, while assuming $m_{CT} = 0.1$ mg, $F_{drag} = 0$ N, $v_0 = 1$ m/s, $L_{ext} = 0.48\ \mu$F and $R_c = 20$ mΩ. Fixed C_{acc} ($400\,\mu$F / $100\,\mu$F) is used to limit V_{acc} (20 kV/40 kV) within $E_{acc} \leqq 80$ kJ in each scan.

calculation is shown in Fig. 9(c), and $R_c = 30\ \mathrm{m}\Omega$, $m_{CT} = 0.1$ mg, $L_{ext} = 0.5\,\mu$H are assumed. The parameter $I_{max}/(\alpha B_{01})$ should be larger than one to avoid the blowby phenomenon because αB_{01} gives the least I_{form} (see Eq. (13)), and this is less than one in the case of SPICA mk. I. Since I_{form} is a function of Δd (see Eq. (9)), it is effective to remove the formation inner-electrode to extend the gap distance as shown in Fig. 9(d). The parameters calculated for this "one-stage electrode", while remaining other conditions the same as "two-stage electrode", are also shown in Fig. 10. In this case, $I_{max}/(\alpha B_{01})$ is about two and large enough to avoid the blowby phenomenon. The optimization results for both one-stage and two-stage electrodes are depicted in Fig. 11. The maximum efficiency of the one-stage electrode is larger than that of the two-stage electrode, although the relation reverses at larger C_{acc} (or smaller V_{acc}). This results mean that only if the blowby phenomenon were not to be expected, the two-stage electrode still has a merit of large ε as long as V_{acc} is limited.

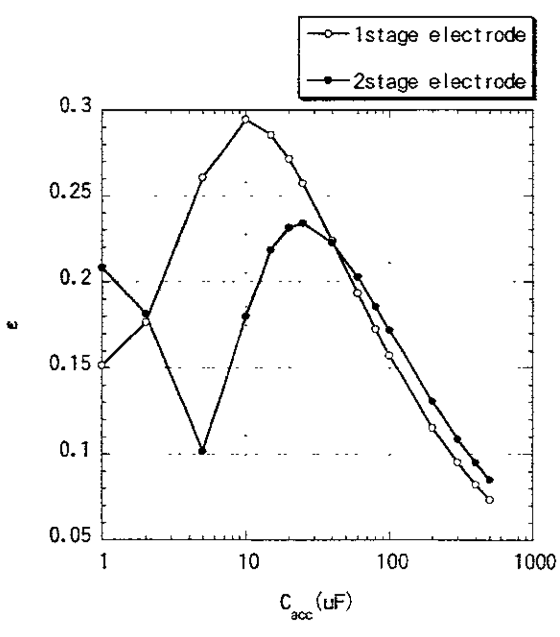

Fig. 11 The optimization results of one-stage electrode and two-stage electrode. Each electrode assumed in this optimization is shown in Fig. 9(c) or (d), and $E_{acc} = 80$ kJ, $R_c = 0.02\ \Omega$, $L_{ext} = 0.48\,\mu$H, $F_{drag} = 0$ N, $v_0 = 1$ m/s are assumed.

Up to this point, the CT mass is fixed to 0.1 mg. Here, let us examine the dependence of ε on m_{CT}. Scanning m_{CT} for the case of one-stage electrode, Fig. 12 is obtained. The E_{acc} is used as a parameter while the others such as C_{acc} (= 400 μF), R_c (= 30 mΩ) and L_{ext} (= 0.5 μH) are fixed. In this case, there is a optimum m_{CT} that maximizes ε for each E_{acc}. The CT mass is controllable with the fuel-gas amount injected into the formation part. As can be seen in Fig. 12, ε is expected to be about 16 % for the one-stage operation. Thus, $E_{CT} \sim 13$ kJ with $m_{CT} \sim 1$ mg is achievable even when a compact capacitor bank of 20 kV - 80 kJ is used. Larger ε and E_{CT} can be achieved by reducing R_c and L_{ext}, or increasing V_{acc}.

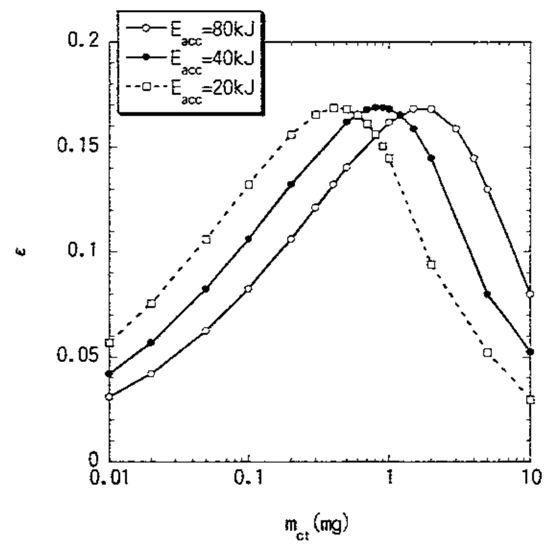

Fig. 12 The mass dependence of ε for one-stage electrode, where $R_c = 0.02\ \Omega$ and $C_{acc} = 400\ \mu$F. Three curves correspond to different E_{acc} of 20 kJ, 40 kJ, and 80 kJ. The other parameters used here are identical to that used in Fig. 11.

6. Summary

A point model of CT acceleration in co-axial electrode has been solved using the fourth-order Runge-Kutta method to obtain the optimum design of a CT injector. It was revealed that the ratio of electrode inductance to external inductance determines the acceleration efficiency. The high efficiency CT injector can be realized by reduction in the external inductance and enlargement of the volume inside the injector to increase the electrode inductance Adiabatic heating of CTs using conical accelerator is also proposed. A conical electrode realizes the high temperature and the long lifetime of CT, as well as the large electrode inductance The conditions to avoid the blowby phenomenon are introduced and applied to the design of the CT formation part. The optimum design is obtained by scanning various parameters for given conditions.

More than 34 % of acceleration efficiency and about 15 kJ of CT kinetic energy are expected with a long (3.2 m) acceleration electrode. This is enough to carry out the CT injection into LHD, although other difficulties such as impurity problems and technological issues for assembling are to be solved. Moderate length of 1.6 m electrode results in the less CT kinetic energy of 7.5 kJ in the optimum condition, but still available for CT injection into LHD plasmas with 1.5 T magnetic field. Our experimental scenario adopts the shortest 0.8m electrode as the first step Although only small acceleration efficiency of 15.7 % is expected for our first CT injector SPICA mk. I, this compact injector is useful to study the basic techniques of CT formation and acceleration. The possibility of one-stage operation is also pointed out in this paper. Only one power supply is needed in this operation. A simple modification of the injector configuration (removal of formation inner-electrode) will be necessary for this one-stage operation to avoid the blowby phenomenon.

Acknowledgement

The authors would like to thank Dr. R. Raman and JFT-2M group for fruitful discussions on technical problems of the CT experiments. The authors would appreciate the continuous supports by Dr. Motojima and LHD experiment group.

References

[1] K. Thomassen *et al.*: Fusion Tech. **34** (1998) 86.
[2] R. Raman *et al.*: Phys. Rev. Lett **73** (1994) 3101.
[3] M. R. Brown and P. M. Bellan: Nucl. Fusion **32** (1992) 1125.
[4] J. Yee and P. M. Bellan: Nucl. Fusion **38** (1998) 711.
[5] J. H. Hammer, J. L. Eddleman, C W Hartman, H. S. McLean and A. W. Molvik: Phys. Fluids B **3** (1991) 2236.
[6] J. Eddleman *et al.*, "Final Report on the LLNL Compact Torus Acceleration Project", UCRL-ID-120238, Lawrence Livermore National Laboratory (Mar 1995).
[7] J. H. Hammer, C. W. Hartman, J. L. Eddleman, H. S. McLean· Phys. Rev Letters **61** (1988) 2843.
[8] Charles W. Hartman and James H. Hammer· Phys. Rev. Lett. **48** (1982) 929.
[9] P. B. Parks Phys. Rev. Lett. **61** (1988) 1364.
[10] W. A. Newcomb: Phys. Fluids B **3** (1991) 1818.
[11] L. J. Perkins, S. K. Ho and J H. Hammer. Nucl. Fusion **28** (1988) 1365
[12] R. J. Hawryluk *et al.*: *Proc. 11th Int. Conf. Plasma Physics and Controlled Nuclear Fusion Research, Kyoto, Japan, 1986* (International Atomic Energy Agency, 1987), Vol.1, p.51.
[13] M.Greenwald *et al.*: Phys. Rev Lett. **61** (1988) 1105.
[14] O. Gehre *et al.*: Phys. Rev. Lett **60** (1988) 1502.
[15] P. Gohil, K. H. Burrell and T H Osborne Nucl. Fusion **38** (1998) 425.
[16] Y. Koide, K H Burrell, B. W. Rice and T. Fujita: Plasma Phys. Control. Fusion **40** (1998) 97.
[17] K. Ida, S.-I. Itoh, K. Itoh, S. Hidekuma, Y. Miura, H. Kawashima, M. Mori, T. Matsuda, N. Suzuki, H. Tamai, T. Yamauchi and JFT-2M Group: Phys. Rev. Lett. **68** (1992) 182.
[18] M. N. Rosenbruth and M. N. Bussac: Nucl. Fusion **19** (1979) 489.
[19] J. Miyazawa. H. Yamada and O. Motojima· "Possibility of Profile Control using Compact Toroid Injection on Large Helical Device", Jpn. J. Appl. Phys. **37** (1998) 6620
[20] S. V. Bozhokin· Sov. J. Plasma Phys. **16** (1990) 702.
[21] C. Xiao, A. Hirose and W. Zawalski: Nucl. Fusion **38** (1998) 249.
[22] M. Fujiwara *et al.*: J. Fusion Energy **15** (1996) 7.
[23] O. Motojima *et al.*: Physics of Plasmas **6** (1999) 1843.
[24] Y. Ono, R. A. Ellis, Jr., A. C. Janos, F. M. Levinton. R. M. Mayo, R. W. Motley. Y. Ueda and M. Yamada: Phys. Rev. Lett **61** (1988) 2847.
[25] T. R. Jarboe. F. J. Wysocki, J. C. Fernández, I. Henins and G. J. Marklin· Phys. Fluids B **2** (1990) 1342.
[26] V. E. Golant. *Proc. of 11th European Conf. on Plasma Phys. and Controlled Fusion,* Aachen (1983), Plasma Phys and Controlled Fusion **26** (1984) 77.

[27] K. Bol, R. A. Ellis *et al.*: Phys. Rev. Letters **29** (1972) 1495.
[28] K. Bol, J. L. Cecchi *et al.*: *Proc. of 5th Int. Conf. on Plasma Phys. and Controlled Nucl. Fusion Research,* Tokyo (1974), Vol. 1, p.83.
[29] R. A. Ellis, H. P. Eubank *et al.*: Nucl. Fusion **16** (1976) 524.
[30] C. W. Barnes *et al.*: Phys. Fluids **29** (1986) 3415.
[31] C. W. Barnes *et al.*: Phys. Fluids B **2** (1990) 1871.
[32] M. R. Brown. D. M. Cutrer and P. M. Bellan: Phys. Fluids B **3** (1991) 1198.
[33] J. B. Taylor: Phys. Rev. Letters **29** (1972) 1495.

Recent Issues of NIFS Series

NIFS-551 T Kuroda H Sugama, R Kanno, M Okamoto and W Horton,
Initial Value Problem of the Toroidal Ion Temperature Gradient Mode , June 1998

NIFS-552 T Mutoh, R. Kumazawa, T Seki, F Simpo, G Nomura, T Ido and T Watari,
Steady State Tests of High Voltage Ceramic Feedthoughs and Co-Axial Transmission Line of ICRF Heating System for the Large Helical Device ; June 1998

NIFS-553 N Noda, K Tsuzuki, A Sagara, N Inoue, T. Muroga,
oronaization in Future Devices -Protecting Layer against Tritium and Energetic Neutrals- July 1998

NIFS-554 S Murakami and H Saleem,
Electromagnetic Effects on Rippling Instability and Tokamak Edge Fluctuations, July 1998

NIFS-555 H Nakamura , K. Ikeda and S. Yamaguchi,
Physical Model of Nernst Element; Aug 1998

NIFS-556 H Okumura, S. Yamaguchi, H. Nakamura, K Ikeda and K Sawada,
Numerical Computation of Thermoelectric and Thermomagnetic Effects, Aug. 1998

NIFS-557 Y Takeiri, M. Osakabe, K. Tsumori, Y. Oka, O. Kaneko, E. Asano, T. Kawamoto, R Akiyama and M. Tanaka,
Development of a High-Current Hydrogen-Negative Ion Source for LHD-NBI System, Aug.1998

NIFS-558 M Tanaka, A. Yu Grosberg and T. Tanaka,
Molecular Dynamics of Structure Organization of Polyampholytes, Sep 1998

NIFS-559 R. Horiuchi, K. Nishimura and T Watanabe,
Kinetic Stabilization of Tilt Disruption in Field-Reversed Configurations, Sep. 1998
(IAEA-CN-69/THP1/11)

NIFS-560 S Sudo, K Kholopenkov, K Matsuoka, S Okamura, C. Takahashi, R. Akiyama, A Fujisawa, K. Ida, H. Idei, H. Iguchi, M. Isobe, S Kado, K. Kondo, S. Kubo, H. Kuramoto, T Minami, S. Morita, S. Nishimura, M. Osakabe, M. Sasao, B. Peterson, K Tanaka, K Toi and Y Yoshimura,
Particle Transport Study with Tracer-Encapsulated Solid Pellet Injection; Oct 1998
(IAEA-CN-69/EXP1/18)

NIFS-561 A Fujisawa, H Iguchi, S. Lee, K. Tanaka, T. Minami, Y. Yoshimura, M Osakabe, K. Matsuoka, S. Okamura, H. Idei, S. Kubo, S Ohdachi, S Morita, R. Akiyama, K Toi, H Sanuki, K Itoh, K. Ida, A Shimizu, S Takagi, C. Takahashi, M Kojima, S Hidekuma, S Nishimura, M. Isobe, A Ejiri, N. Inoue, R Sakamoto, Y Hamada and M Fujiwara,
Dynamic Behavior Associated with Electric Field Transitions in CHS Heliotron/Torsatron, Oct 1998
(IAEA-CN-69/EX5/1)

NIFS-562 S. Yoshikawa,
Next Generation Toroidal Devices; Oct 1998

NIFS-563 Y. Todo and T Sato,
Kinetic-Magnetohydrodynamic Simulation Study of Fast Ions and Toroidal Alfvén Eigenmodes; Oct 1998
(IAEA-CN-69/THP2/22)

NIFS-564 T Watari, T Shimozuma, Y. Takeiri, R Kumazawa, T Mutoh, M Sato, O. Kaneko, K. Ohkubo, S Kubo, H. Idei, Y Oka, M Osakabe, T Seki, K Tsumori, Y Yoshimura, R. Akiyama, T Kawamoto, S Kobayashi, F Shimpo, Y Takita, E Asano, S Itoh, G Nomura, T. Ido, M. Hamabe, M Fujiwara, A. Iiyoshi, S Morimoto, T Bigelow and Y.P Zhao,
Steady State Heating Technology Development for LHD, Oct 1998
(IAEA-CN-69/FTP/21)

NIFS-565 A Sagara, K.Y. Watanabe, K. Yamazaki, O Motojima, M Fujiwara, O Mitarai, S. Imagawa, H Yamanishi, H. Chikaraishi, A Kohyama, H. Matsui, T. Muroga, T Noda, N Ohyabu, T Satow, A A Shishkin, S Tanaka, T Terai and T Uda,
LHD-Type Compact Helical Reactors; Oct 1998
(IAEA-CN-69/FTP/03(R)

NIFS-566 N. Nakajima, J Chen, K. Ichiguchi and M Okamoto,
Global Mode Analysis of Ideal MHD Modes in L=2 Heliotron/Torsatron Systems, Oct 1998
(IAEA-CN-69/THP1/08)

NIFS-567 K. Ida, M. Osakabe, K Tanaka, T. Minami, S. Nishimura, S Okamura, A Fujisawa, Y. Yoshimura, S. Kubo, R Akiyama, D.S.Darrow, H Idei, H Iguchi, M Isobe, S Kado, T. Kondo, S. Lee, K Matsuoka, S Morita, I Nomura, S Ohdachi, M Sasao, A

Shimizu, K. Tumon, S Takayama, M. Takechı, S. Takagı, C Takahashı, K. Toı and T Watari,
Transition from L Mode to High Ion Temperature Mode in CHS Heliotron/Torsatron Plasmas, Oct 1998
(IAEA-CN-69/EX2/2)

NIFS-568 S. Okamura, K. Matsuoka, R. Akiyama, D.S. Darrow, A. Ejiri, A. Fujisawa, M. Fujıwara, M. Goto, K. Ida H. Idei, H Iguchı, N. Inoue, M. Isobe, K. Itoh, S. Kado, K. Khlopenkov, T. Kondo, S. Kubo, A. Lazaros, S. Lee, G. Matsunaga, T. Minamı, S. Monta, S. Murakami, N. Nakajima, N. Nikai, S. Nishimura, I. Nomura, S. Ohdachi, K. Ohkunı, M. Osakabe, R. Pavlichenko, B. Peterson, R. Sakamoto, H. Sanuki, M. Sasao, A. Shimizu, Y. Shirai, S. Sudo, S. Takagı, C. Takahashı, S. Takayama, M. Takechı, K. Tanaka, K. Toi, K. Yamazakı, Y. Yoshimura and T. Watari,
Confinement Physics Study in a Small Low-Aspect-Ratio Helical Device CHS, Oct 1998
(IAEA-CN-69/OV4/5)

NIFS-569 M.M. Skoric, T. Sato, A. Maiuckov, M.S. Jovanovic,
Micro- and Macro-scale Self-organization in a Dissipative Plasma; Oct. 1998

NIFS-570 T. Hayashi, N. Mizuguchi, T-H. Watanabe, T. Sato and the Complexity Simulation Group,
Nonlinear Simulations of Internal Reconnection Event in Spherical Tokamak; Oct 1998
(IAEA-CN-69/TH3/3)

NIFS-571 A. Iiyoshı, A Komori, A. Ejiri, M. Emoto, H. Funaba, M. Goto, K. Ida, H. Idei, S. Inagakı, S. Kado, O Kaneko, K Kawahata, S. Kubo, R. Kumazawa, S Masuzakı, T. Minamı, J. Miyazawa, T. Morisakı, S. Monta, S. Murakami, S. Muto, T. Muto, Y Nagayama, Y. Nakamura, H. Nakanishi, K. Narihara, K. Nishimura, N. Noda, T. Kobuchi, S. Ohdachi, N. Ohyabu, Y. Oka, M. Osakabe, T. Ozaki, B.J. Peterson, A. Sagara, S. Sakakibara, R. Sakamoto, H. Sasao, M. Sasao, K. Sato, M. Sato, T. Sekı, T Shimozuma, M. Shoji, H. Suzukı, Y. Takeiri, K. Tanaka, K. Toi, T. Tokuzawa, K. Tsumori, I. Yamada, H. Yamada, S. Yamaguchi, M. Yokoyama, K.Y.Watanabe, T. Watarı, R. Akiyama, H. Chikaraishi, K. Haba, S. Hamaguchi, S. Iima, S. Imagawa, N. Inoue, K. Iwamoto, S Kitagawa, Y. Kubota, J. Kodaira, R Maekawa, T Mito. T Nagasaka, A. Nishımura, Y. Takita, C. Takahashi. K Takahata, K. Yamauchı, H Tamura, T. Tsuzuki, S Yamada, N. Yanagı, H. Yonezu, Y Hamada, K. Matsuoka, K. Muraı, K. Ohkubo. I. Ohtake. M. Okamoto, S Sato, T. Satow, S. Sudo, S. Tanahashı, K Yamazaki, M. Fujiwara and O. Motojima,
An Overview of the Large Helical Device Project; Oct. 1998
(IAEA-CN-69/OV1/4)

NIFS-572 M. Fujıwara, H Yamada, A Ejın, M Emoto, H. Funaba, M. Goto, K. Ida, H Ideı, S Inagakı, S Kado, O Kaneko, K Kawahata, A. Komorı, S. Kubo, R. Kumazawa, S Masuzakı, T. Minami, J. Miyazawa, T Morisakı, S. Monta, S Murakamı, S Muto, T Muto, Y. Nagayama, Y. Nakamura, H. Nakanıshı, K. Narihara, K. Nishımura, N Noda, T Kobuchı, S. Ohdachi, N. Ohyabu, Y. Oka, M. Osakabe, T. Ozakı, B. J. Peterson, A. Sagara, S. Sakakıbara, R. Sakamoto, H. Sasao, M Sasao, K. Sato, M. Sato, T Sekı, T. Shımozuma, M. Shoji, H. Sazukı, Y Takeiri, K. Tanaka, K. Toi, T. Tokuzawa, K. Tsumori, I. Yamada, S. Yamaguchi, M. Yokoyama, K.Y. Watanabe, T. Watari, R. Akiyama, H. Chıkaraıshı, K. Haba, S. Hamaguchi, M. Iima, S. Imagawa, N Inoue, K. Iwamoto, S. Kitagawa, Y Kubota, J. Kodaıra, R. Maekawa, T Mito, T. Nagasaka, A. Nishımura, Y. Takita, C Takahashi, K. Takahata, K. Yamauchı, H. Tamura, T. Tsuzuki, S. Yamada, N. Yanagi, H. Yonezu, Y. Hamada, K. Matsuoka, K Murai, K. Ohkubo, I Ohtake, M Okamoto, S. Sato, T. Satow, S. Sudo, S. Tanahashi, K. Yamazaki, O. Motojıma and A. Iiyoshı,
Plasma Confinement Studies in LHD; Oct. 1998
(IAEA-CN-69/EX2/3)

NIFS-573 O. Motojima, K. Akaishı, H. Chikaraishi, H. Funaba, S. Hamaguchi, S. Imagawa, S. Inagaki, N. Inoue, A. Iwamoto, S. Kitagawa, A. Komori, Y. Kubota, R Maekawa, S. Masuzaki, T. Mito, J. Miyazawa, T. Morisaki, T. Muroga, T. Nagasaka, Y. Nakmura, A. Nıshımura, K. Nishımura, N. Noda, N. Ohyabu, S. Sagara, S. Sakakibara, R. Sakamoto, S. Satoh, T. Satow, M. Shoji, H Suzuki, K. Takahata, H. Tamura, K. Watanabe, H. Yamada, S. Yamada, S. Yamaguchi, K. Yamazaki, N. Yanagi, T Baba, H. Hayashi, M. Iima, T Inoue, S. Kato, T Kato, T. Kondo, S. Moriuchi, H. Ogawa, I. Ohtake, K. Ooba, H. Sekiguchi, N. Suzukı, S. Takamı, Y. Tanıguchi, T. Tsuzuki, N Yamamoto, K. Yasuı, H. Yonezu, M. Fujıwara and A. Iıyoshi,
Progress Summary of LHD Engineering Design and Construction; Oct. 1998
(IAEA-CN-69/FT2/1)

NIFS-574 K. Toı, M Takechı, S. Takagi, G. Matsunaga, M. Isobe, T. Kondo, M. Sasao, D.S Darrow, K. Ohkunı, S Ohdachı, R. Akıyama A. Fujisawa, M. Gotoh, H. Idei, K. Ida, H. Iguchı, S. Kado, M. Kojima, S. Kubo, S. Lee, K. Matsuoka, T. Minami, S. Morita, N. Nikaı, S. Nishimura, S. Okamura, M. Osakabe, A. Shimizu, Y. Shiraı, C. Takahashi, K. Tanaka, T. Watarı and Y. Yoshımura,
Global MHD Modes Excited by Energetic Ions in Heliotron/Torsatron Plasmas, Oct. 1998
(IAEA-CN-69/EXP1/19)

NIFS-575 Y Hamada, A Nishizawa, Y. Kawasumı, A. Fujisawa, M. Kojıma, K. Narihara, K. Ida, A. Ejin, S. Ohdachı, K. Kawahata, K Toı, K. Sato, T. Seki, H. Iguchı, K. Adachı, S. Hidekuma, S.Hirokura, K. Iwasaki, T. Ido, R. Kumazawa, H. Kuramoto, T. Mınamı, I.. Nomura, M. Sasao, K.N. Sato, T. Tsuzukı, I. Yamada and T. Watarı,
Potential Turbulence in Tokamak Plasmas; Oct. 1998
(IAEA-CN-69/EXP2/14)

NIFS-576 S. Murakami, U. Gasparino, H. Idei, S. Kubo, H. Maassberg, N. Marushchenko, N. Nakajima, M. Romé and M. Okamoto,
5D Simulation Study of Suprathermal Electron Transport in Non-Axisymmetric Plasmas; Oct. 1998
(IAEA-CN-69/THP1/01)

NIFS-577 S. Fujiwara and T. Sato,
Molecular Dynamics Simulation of Structure Formation of Short Chain Molecules; Nov. 1998

NIFS-578 T. Yamagishi,
Eigenfunctions for Vlasov Equation in Multi-species Plasmas Nov. 1998

NIFS-579 M Tanaka, A Yu Grosberg and T Tanaka,
Molecular Dynamics of Strongly-Coupled Multichain Coulomb Polymers in Pure and Salt Aqueous Solutions, Nov 1998

NIFS-580 J Chen, N Nakajima and M Okamoto,
Global Mode Analysis of Ideal MHD Modes in a Heliotron/Torsatron System. I Mercier-unstable Equilibria, Dec 1998

NIFS-581 M Tanaka, A. Yu Grosberg and T Tanaka,
Comparison of Multichain Coulomb Polymers in Isolated and Periodic Systems: Molecular Dynamics Study; Jan 1999

NIFS-582 V S Chan and S Murakami,
Self-Consistent Electric Field Effect on Electron Transport of ECH Plasmas; Feb 1999

NIFS-583 M Yokoyama, N. Nakajima, M. Okamoto, Y. Nakamura and M Wakatani,
Roles of Bumpy Field on Collisionless Particle Confinement in Helical-Axis Heliotrons; Feb 1999

NIFS-584 T-H Watanabe, T Hayashi, T Sato, M Yamada and H. Ji,
Modeling of Magnetic Island Formation in Magnetic Reconnection Experiment; Feb 1999

NIFS-585 R. Kumazawa, T. Mutoh, T. Seki, F. Shinpo, G Nomura, T Ido, T. Watari, Jean-Marie Noterdaeme and Yangping Zhao,
Liquid Stub Tuner for Ion Cyclotron Heating; Mar. 1999

NIFS-586 A Sagara, M. Iima, S Inagaki, N. Inoue, H. Suzuki, K. Tsuzuki, S Masuzaki, J Miyazawa, S. Morita, Y Nakamura, N. Noda, B. Peterson, S Sakakibara, T. Shimozuma, H Yamada, K Akaishi, H Chikaraishi, H Funaba, O Kaneko, K Kawahata, A Komori, N. Ohyabu, O Motojima, LHD Exp. Group 1, LHD Exp. Group 2,
Wall Conditioning at the Starting Phase of LHD, Mar. 1999

NIFS-587 T. Nakamura and T. Yabe,
Cubic Interpolated Propagation Scheme for Solving the Hyper-Dimensional Vlasov-Poisson Equation in Phase Space; Mar 1999

NIFS-588 W.X Wnag, N. Nakajima, S. Murakami and M. Okamoto,
An Accurate δf Method for Neoclassical Transport Calculation, Mar. 1999

NIFS-589 K. Kishida, K. Araki, S. Kishiba and K Suzuki,
Local or Nonlocal? Orthonormal Divergence-free Wavelet Analysis of Nonlinear Interactions in Turbulence, Mar 1999

NIFS-590 K Araki, K. Suzuki, K Kishida and S Kishiba,
Multiresolution Approximation of the Vector Fields on T^3, Mar. 1999

NIFS-591 K. Yamazaki, H. Yamada, K.Y Watanabe, K. Nishimura, S. Yamaguchi, H Nakanishi, A. Komori, H. Suzuki, T. Mito, H. Chikaraishi, K. Murai, O. Motojima and the LHD Group,
Overview of the Large Helical Device (LHD) Control System and Its First Operation, Apr 1999

NIFS-592 T Takahashi and Y Nakao,
Thermonuclear Reactivity of D-T Fusion Plasma with Spin-Polarized Fuel, Apr 1999

NIFS-593 H. Sugama,
Damping of Toroidal Ion Temperature Gradient Modes, Apr 1999

NIFS-594 Xiaodong Li,
Analysis of Crowbar Action of High Voltage DC Power Supply in the LHD ICRF System, Apr. 1999

NIFS-595 K. Nishimura, R Horiuchi and T Sato,
Drift-kink Instability Induced by Beam Ions in Field-reversed Configurations, Apr. 1999

NIFS-596 Y Suzuki, T-H. Watanabe, T. Sato and T Hayashi,
Three-dimensional Simulation Study of Compact Toroid Plasmoid Injection into Magnetized Plasmas; Apr 1999

NIFS-597 H. Sanuki, K. Itoh, M. Yokoyama, A. Fujisawa, K. Ida, S. Toda, S.-I Itoh, M. Yagi and A Fukuyama,

Possibility of Internal Transport Barrier Formation and Electric Field Bifurcation in LHD Plasma; May 1999

NIFS-598 S. Nakazawa, N. Nakajima, M. Okamoto and N. Ohyabu,
One Dimensional Simulation on Stability of Detached Plasma in a Tokamak Divertor; June 1999

NIFS-599 S. Murakami, N. Nakajima, M. Okamoto and J. Nhrenberg,
Effect of Energetic Ion Loss on ICRF Heating Efficiency and Energy Confinement Time in Heliotrons; June 1999

NIFS-600 R. Horiuchi and T Sato,
Three-Dimensional Particle Simulation of Plasma Instabilities and Collisionless Reconnection in a Current Sheet;; June 1999

NIFS-601 W. Wang, M Okamoto, N Nakajima and S Murakami,
Collisional Transport in a Plasma with Steep Gradients, June 1999

NIFS-602 T. Mutoh, R. Kumazawa, T. Saki, K. Saito, F. Simpo, G. Nomura, T. Watari, X. Jikang, G. Cattanei, H. Okada, K. Ohkubo, M. Sato, S. Kubo, T. Shimozuma, H. Idei, Y. Yoshimura, O. Kaneko, Y. Takeiri, M. Osakabe, Y. Oka, K. Tsumori, A. Komori, H. Yamada, K. Watanabe, S. Sakakibara, M. Shoji, R. Sakamoto, S. Inagaki, J. Miyazawa, S. Morita, K. Tanaka, B.J. Peterson, S. Murakami, T. Minami, S. Ohdachi, S. Kado, K. Narihara, H. Sasao, H. Suzuki, K. Kawahata, N. Ohyabu, Y Nakamura, H. Funaba, S. Masuzaki, S. Muto, K. Sato, T. Morisaki, S. Sudo, Y Nagayama, T. Watanabe, M. Sasao, K.. Ida, N. Noda, K. Yamazaki, K. Akaishi, A. Sagara, K. Nishimura, T. Ozaki, K. Toi, O. Motojima, M. Fujiwara, A Iiyoshi and LHD Exp. Group 1 and 2,
First ICRF Heating Experiment in the Large Helical Device; July 1999

NIFS-603 P.C. de Vries, Y. Nagayama, K. Kawahata, S. Inagaki, H. Sasao and K. Nagasaki,
Polarization of Electron Cyclotron Emission Spectra in LHD; July 1999

NIFS-604 W Wang, N. Nakajima, M Okamoto and S. Murakami,
δf Simulation of Ion Neoclassical Transport; July 1999

NIFS-605 T Hayashi, N. Mizuguchi, T. Sato and the Complexity Simulation Group,
Numerical Simulation of Internal Reconnection Event in Spherical Tokamak, July 1999

NIFS-606 M. Okamoto, N Nakajima and W Wang,
On the Two Weighting Scheme for δf Collisional Transport Simulation; Aug. 1999

NIFS-607 O. Motojima, A.A. Shishkin, S. Inagaki, K. Y. Watanabe,
Possible Control Scenario of Radial Electric Field by Loss-Cone-Particle Injection into Helical Device; Aug. 1999

NIFS-608 R. Tanaka, T Nakamura and T. Yabe,
Constructing Exactly Conservative Scheme in Non-conservative Form, Aug. 1999

NIFS-609 H. Sugama,
Gyrokinetic Field Theory; Aug. 1999

NIFS-610 M. Takechi, G. Matsunaga, S Takagi, K.Ohkuni, K. Toi, M. Osakabe, M Isobe, S Okamura, K. Matsuoka, A Fujisawa, H Iguchi, S. Lee, T. Minami, K. Tanaka, Y Yoshimura and CHS Group,
Core Localized Toroidal Alfven Eigenmodes Destabilized By Energetic Ions in the CHS Heliotron/Torsatron, Sep. 1999

NIFS-611 K. Ichiguchi,
MHD Equilibrium and Stability in Heliotron Plasmas, Sep 1999

NIFS-612 Y Sato, M Yokoyama, M Wakatani and V D. Pusovitov,
Complete Suppression of Pfirsch-Schluter Current in a Toroidal l=3 Stellarator; Oct. 1999

NIFS-613 S. Wang, H. Sanuki and H. Sugama,
Reduced Drift Kinetic Equation for Neoclassical Transport of Helical Plasmas in Ultra-low Collisionality Regime; Oct. 1999

NIFS-614 J. Miyazawa, H. Yamada, K. Yasui, S. Kato, N., Fukumoto, M. Nagata and T Uyama,
Design of Spheromak Injector Using Conical Accelerator for Large Helical Device, Nov. 1999